

RSC Advances

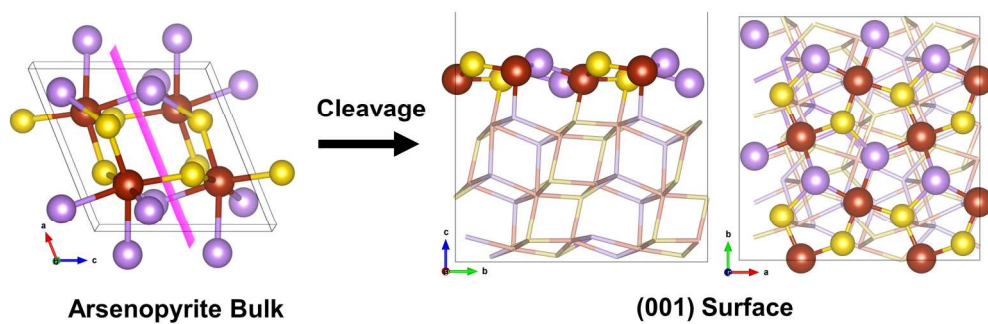


This is an *Accepted Manuscript*, which has been through the Royal Society of Chemistry peer review process and has been accepted for publication.

Accepted Manuscripts are published online shortly after acceptance, before technical editing, formatting and proof reading. Using this free service, authors can make their results available to the community, in citable form, before we publish the edited article. This *Accepted Manuscript* will be replaced by the edited, formatted and paginated article as soon as this is available.

You can find more information about *Accepted Manuscripts* in the [Information for Authors](#).

Please note that technical editing may introduce minor changes to the text and/or graphics, which may alter content. The journal's standard [Terms & Conditions](#) and the [Ethical guidelines](#) still apply. In no event shall the Royal Society of Chemistry be held responsible for any errors or omissions in this *Accepted Manuscript* or any consequences arising from the use of any information it contains.



Graphical Abstract
190x142mm (300 x 300 DPI)

Electronic and structural properties of arsenopyrite bulk and its cleavage surfaces – A DFT study.

Juliana C. M. Silva, Heitor A. De Abreu, Hélio A. Duarte*

Grupo de Pesquisa em Química Inorgânica Teórica – GPQIT –
Departamento de Química, ICEX, Universidade Federal de Minas Gerais
(UFMG), Av. Antônio Carlos, 6627, 31270-901 Belo Horizonte, MG, Brazil

***Corresponding author: Hélio A. Duarte**

duarteh@ufmg.br

Abstract

Arsenopyrite is the most abundant arsenic containing mineral on earth and it is normally associated with many other minerals of economic importance. Therefore, it is involved in environmental impacts of mining activities. The bonding nature of arsenopyrite and its preferential cleavage surface are still controversial. In the present work we have investigated the structural and electronic properties of arsenopyrite and its surfaces formation using density functional/plane waves method. Quantum theory of atoms in molecules (QTAIM) and electron localization function (ELF) were applied for investigating the nature of the bonding in arsenopyrite. No evidence was found for Fe–Fe bonding in the bulk structure. The As-S bond has large covalent character and it is unexpected to be broken in the surface formation. The cleavage and surface energies have been calculated indicating that (001) surface is the most favored to be formed.

Key-words: Arsenopyrite, DFT, Cleavage Surface, Plane Waves, QTAIM

1. Introduction

Arsenopyrite is a mineral sulfide commonly found in the nature associated to noble metals such as gold, copper and silver. This mineral has little economic value [1] and the mining process generates huge quantity of tailings which are disposed in dams [2]. The exposition of sulfide minerals, such as arsenopyrite, to the environment normally leads to acid rock drainage (ARD).

In the ARD process, the mineral sulfides present in mining tailings oxidize producing in the final process sulfuric acid. The generated solution acts as a leaching agent, i.e., as a mixture that solubilizes the solid mineral constituents, producing an acidic solution containing dissolved metals, which can contaminate soil and underground water. The ARD is a spontaneous process that arises where the rock is exposed to air and moisture. A classic example occurs in Rio Tinto in Spain [3]. Along this river there is a large deposit of pyrite and the process of ARD has lasted for centuries, leading to pH of about 2 with high concentration of heavy metals. But ARD normally occurs due to anthropogenic activities, such as mining, that exposes large amount of sulfide minerals to the atmosphere [4].

Although arsenopyrite is stable under reducing conditions, its oxidation due to weathering effects releases sulfates, arsenites (As(III)) and arsenates (As(V)) species [1] to the environment. The arsenic released due to arsenopyrite oxidation is an environmental hazard and may become a health problem [5]. The understanding of the kinetic and the mechanism of dissolution of this material in different conditions is essential for assessing the stability of the arsenic containing tailings and the development of more efficient process to control its remobilization with great environmental, social and economic consequences.

There are several studies in the literature concerning the products formed in arsenopyrite oxidation in different media [1, 2, 6-11]. However in many of them the results diverge and there is no consensus concerning the reaction mechanism at a molecular level. In this context, first-principles calculations emerge as a tool providing information about the surface reactivity of arsenopyrite and insights about its oxidation mechanism. For pyrite there are many theoretical studies concerning its cleavage surfaces [12, 13], water

adsorption [14, 15] and mechanism of oxidation [16], as well as about chalcopyrite's surfaces and adsorption of leaching agents [17-20]. Nevertheless, to the best of our knowledge, there is only one theoretical study about the electronic and geometric characteristics of (110) surface of arsenopyrite [21] and also two about arsenic incorporation into pyrite [22, 23]. More information about arsenopyrite and its chemical reactivity is therefore necessary.

Arsenopyrite (ideal formula FeAsS) is the most common arsenic containing mineral on Earth and may be found in many ore deposits. It is a diamagnetic semiconductor [24]. Its unit cell is monoclinic and has space group $P2_1/c$ derived from marcasite (orthorhombic FeS_2) [25] with 4 FeAsS formulas per unit cell, as shown in Figure 1a-b. However, a refinement of the arsenopyrite structure was also accomplished in space group $C2_1/d$ [26], in a pseudo-orthorhombic unit cell, as shown in Figure 1c. Its structure contains arsenic and sulfur dianions (As-S) coordinated to the iron atom in an octahedral shape (Figure 2a). The Fe atoms are coordinated to three As and three S atoms and each anion is coordinated to three iron atoms and another anion in a tetrahedral shape. The FeAs_3S_3 octahedrons are asymmetric and share two opposite edges to form single strips parallel to (10-1) surface (Figure 2b). The adjacent octahedral coordinations in a row are related to each other by an inversion operation, leading to distances between Fe cations alternately short and long. In the direction of the Fe-Fe contact, the short Fe-Fe bond cuts the long S-S edge, whereas the long Fe-Fe bond cuts the short As-As edge. Natural arsenopyrite has a composition ranging from $\text{FeAs}_{0.9}\text{S}_{1.1}$ to $\text{FeAs}_{1.1}\text{S}_{0.9}$ [27] and there may be metal impurity such as Co atom replacing Fe [26] in the structure. Mössbauer spectroscopy indicates that the Fe atom is divalent at the low-spin state, in an octahedral environment [28, 29].

Concerning the favorable cleavage plane, there is no consensus which is the favored plane among (100) [11], (001) [30], (101) [25, 31] and (110) [21, 32] planes. Many of the reported works did not define clearly which is the unit cell used as reference, leading to some ambiguity in defining the favored cleavage.

In the present work, the structural and electronic properties of the arsenopyrite bulk and different cleavage surfaces have been investigated aiming to fulfill the lack of information about this system.

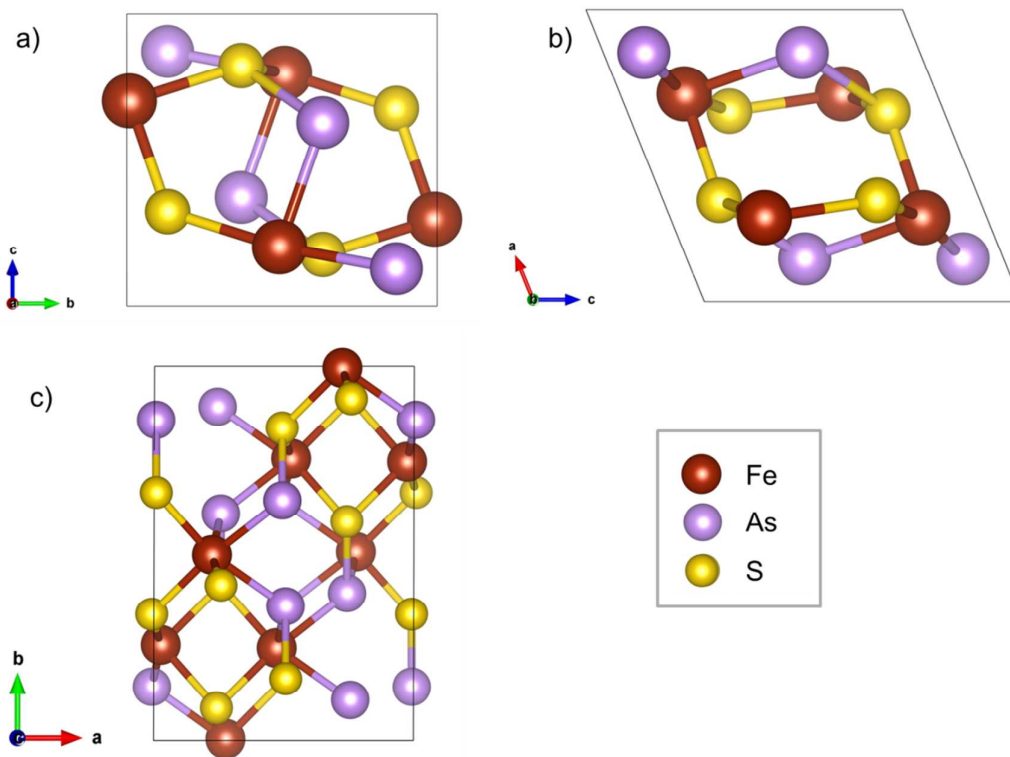


Figure 1: Arsenopyrite structure. a) view of the monoclinic cell along *a* axis; b) view of the monoclinic cell along *b* axis; c) view of the pseudo-orthorhombic cell along *c* axis.

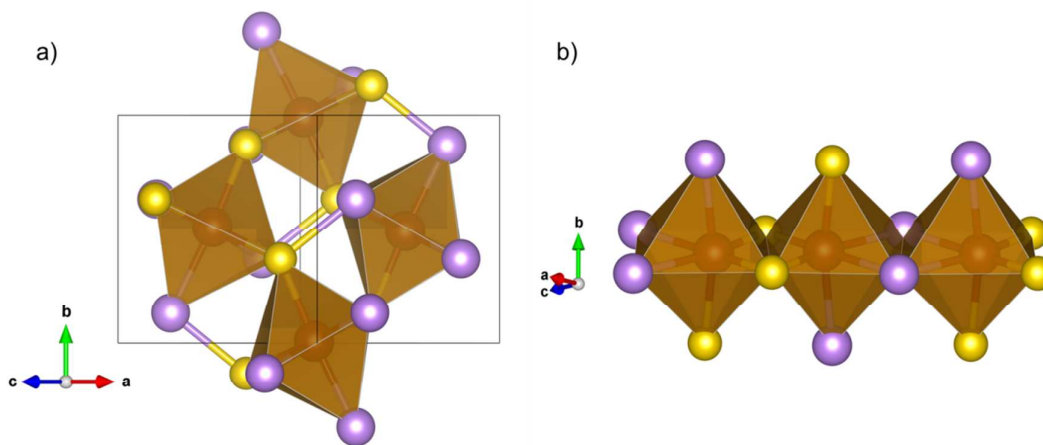


Figure 2: a) As-S dianions octahedrally coordinated to Fe. b) Neighbor octahedrons sharing one edge. Yellow atoms are sulfur, purple are arsenic and red are iron.

2. Methodology

The calculations have been performed based on the density functional theory (DFT)/plane waves methodology with periodic boundary conditions as implemented in the Quantum Espresso package [33]. The PW91[34] exchange/correlation (XC) functional and ultrasoft pseudopotentials proposed by Vanderbilt [35] with the following valence configurations: Fe ($3s^2 3p^6 3d^{6.5} 4s^1 4p^0$), As ($4s^2 4p^3$), S ($3s^2 3p^4$) were used. For the bulk, a cutoff energy of 60 Ry was used and a $4 \times 4 \times 4$ **K**-point mesh sampling based on the Monkhorst-Pack scheme [36] was chosen, besides Marzari-Vanderbilt [37] 0.02 Ry smearing. For the surface, 30 Ry energy cutoff and a $2 \times 2 \times 1$ **K**-point mesh was used. The energy was converged to 10^{-9} Ry. All surfaces were set using a ($2 \times 2 \times 2$) slab model with 15 Å of vacuum.

All calculations were spin compensated. Geometry optimization were carried out using Damped dynamics method [38] with Parrinello-Rahman extended Lagrangian [39], keeping a force tolerance criterion of 10^{-3} Ry Bohr $^{-1}$. The atomic positions, as well as the cell parameters, were fully optimized for bulk. For the slab calculations only the atomic positions were fully optimized.

Bader's QTAIM (Quantum Theory of Atoms In Molecules) method [40] was used to investigate the electronic structure of the solid using the program Critic2 [41]. For bulk modulus calculation, the program Gibbs2 [42] was used. Band structure, density of states (DOS), electron localization function (ELF) and electron density plots were built using Quantum Espresso code using a ($8 \times 8 \times 8$) mesh of **K**-points and for the QTAIM analysis the electron density was built using ($12 \times 12 \times 12$) mesh of **K**-points.

3. Results and discussion

Bulk

The calculated interatomic distances of arsenopyrite bulk are shown on Table 1 and compared with available experimental values. The theoretical estimates are closer to the experimental results of Bindi *et al.* [29] with a maximum of 2% difference, which are more recent and refer to a sample rich in As. The average Fe-S distance is 2.203 Å, 0.028 Å less than the experimental

value [29] and also less than the values calculated using similar methodologies for marcasite (orthorhombic FeS_2) of 2.23 Å [43] and the one of chalcopyrite (CuFeS_2) of 2.241 Å [17], as expected. The average Fe-As distance of 2.402 Å is 0.005 Å larger than the experimental value [29], and the As-S distance of 2.405 Å is 0.031 Å larger. The As-S bond length is also larger than the S-S distance calculated by Gudelli *et al.* [43] for marcasite (2.20 Å), which is expected due to the larger atomic radius of As. Gudelli *et al.* [43] also found only one Fe-Fe distance for marcasite (3.38 Å), an intermediate value between both distances found in the present work.

The cell parameter results after optimization are shown on Table 2. They are in agreement with the experimental data and are closer to these data than the DFT/PBE/plane waves results of Corkhill *et al.* [21]. The differences between lattice parameters did not exceed 0.022 Å, 0.33 degrees in β and 1.72 Å³ in volume, compared to Bindi *et al.* [29].

Table 1: Interatomic distances for arsenopyrite bulk. All values are in angstroms.

| Reference | Short Fe-Fe | Long Fe-Fe | Fe-S | Fe-As | As-S |
|--------------------------|-------------|------------|--|--|-------|
| This work | 2.668 | 3.765 | 2.190; 2.198; 2.222 | 2.380; 2.410; 2.415 | 2.405 |
| Experimental (1961) [27] | 2.82 | 3.62 | 2.22; 2.24; 2.25; 2.26; 2.26; 2.29 | 2.30; 2.32; 2.32; 2.38; 2.39; 2.41 | 2.33 |
| Experimental (1987) [26] | 2.922 | 3.627 | 2.239; 2.250; 2.257 | 2.336; 2.371; 2.375 | 2.346 |
| Experimental (2012) [29] | 2.734 | 3.741 | 2.229; 2.230; 2.233 | 2.370; 2.409; 2.412 | 2.374 |

Table 2: Crystallographic data of arsenopyrite bulk.

| | $a/\text{\AA}$ | $b/\text{\AA}$ | $c/\text{\AA}$ | $\beta/^\circ$ | Volume / \AA^3 |
|-----------------------------|----------------|----------------|----------------|----------------|-------------------------|
| This work | 5.739 | 5.668 | 5.763 | 112.05 | 173.74 |
| DFT/PBE [21] | 5.61 | 5.56 | 5.63 | 111.67 | 164.20 |
| Experimental (1961) [27] | 5.744 | 5.675 | 5.785 | 112.17 | 174.50 |
| Experimental (1987) [26] | 5.741 | 5.649 | 5.756 | 110.59 | 174.73 |
| Experimental (2012) [29] | 5.761 | 5.684 | 5.767 | 111.72 | 175.46 |

Several studies tried to explain the differences in pyrite (cubic FeS_2), marcasite (orthorhombic FeS_2), arsenopyrite (FeAsS) and lollingite (FeAs_2) structures. Hulliger and Mooser [44], Pearson [45] and Nickel [46, 47] used ligand field theory to explain the stabilities of each structure. In pyrite, neighbor octahedrons share common corners, while in the other three sulfides, they share edges. In lollingite, the Fe-Fe distance is shorter than in marcasite, and in arsenopyrite there are alternate short and long distances. In these works, as well as in the works of Brostigen and Kjekshus [48], and Goodenough [49], the iron atom in arsenopyrite was considered to be in the trivalent oxidation state. These authors, except Goodenough [49], considered that there should be a Fe–Fe bond in arsenopyrite to explain the fact that iron is trivalent, but in a low spin state in this mineral, since arsenopyrite is diamagnetic. In fact Pauling [50] has found complexes with Fe–Fe bond up to 2.78 Å long. Vaughan and Craig [28] and Bindi *et al.* [29] showed through Mössbauer spectroscopy that iron is actually in divalent state for all of these sulfides. Tossel *et al.* [51] considered this result and calculated the ionization energy of orbitals in a MA_6 model for sulfides through SCF- X_α -SW method. They concluded that these structures are defined by metal-dianion interaction and proposed an explanation for the different structures based on molecular orbitals occupation. Schmokel and coworkers [52] made a detailed analysis of the experimental and theoretical electron density of pyrite and marcasite. They found that S-S bonds are more covalent and Fe-S bonds are weaker in pyrite compared to marcasite. This is

explained based on the distribution of the *d*-orbital-like density difference between the two polymorphs.

XPS experiments performed by Nesbitt *et al.* [1, 53] checked that in arsenopyrite and lollingite bulk, the iron is divalent because the main peak on the spectra is very close in bonding energy to pyrite's spectra. They also suggested that As and S atoms are in (-1) oxidation state in arsenopyrite. Then, it is accepted that the oxidation states in arsenopyrite are $\text{Fe}^{2+}\text{As}^{-}\text{S}^{-}$.

In order to better understand the electronic properties of arsenopyrite and also validate the bulk model, the band structure was calculated using the **K**-points path suggested by Setyawan *et al.* [54] for a monoclinic cell, see Figure S1. It can be seen by the band structure shown in Figure 3 that arsenopyrite is a semiconductor, according to the literature [55]. The indirect band gap of 0.75 eV from D to Γ point is shown with the red vector. This value is 0.07 eV lower than the experimental value of 0.82 eV [9], as expected, since it is well known that the GGA XC functional underestimates the band gap [56]. The band gap values for pyrite vary from 0.7 to 2.62 eV, but the most reliable ones are between 0.9 and 0.95 eV, measured in photoconductivity experiments [57, 58]. Opahle *et al.* [59] found a value of 0.85 eV in a DFT/LDA-PZ calculation for pyrite, the same difference from experimental values was found for arsenopyrite in the present work. Gudelli *et al.* [43] calculated 1.186 eV band gap for pyrite and 1.603 eV for marcasite using TBmBJ potential [56], which are overestimated.

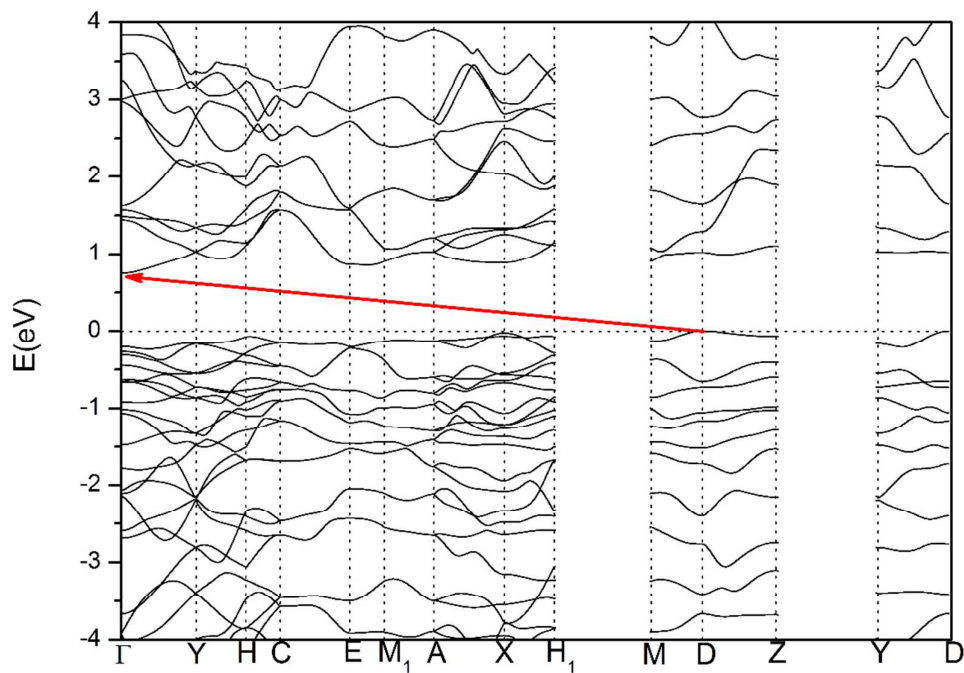


Figure 3: Band structure calculated for arsenopyrite.

The total and projected density of states (DOS) are shown in Figure 4. The iron atom is the one that most contributes to the states around the Fermi level, in both valence and conduction bands, specially the d orbitals of iron (Figure S2). According to the discussion made by De Oliveira and Duarte [17], this characteristic is coherent with an Fe atom in the oxidation state (II) since this atom can be oxidized as well as reduced.

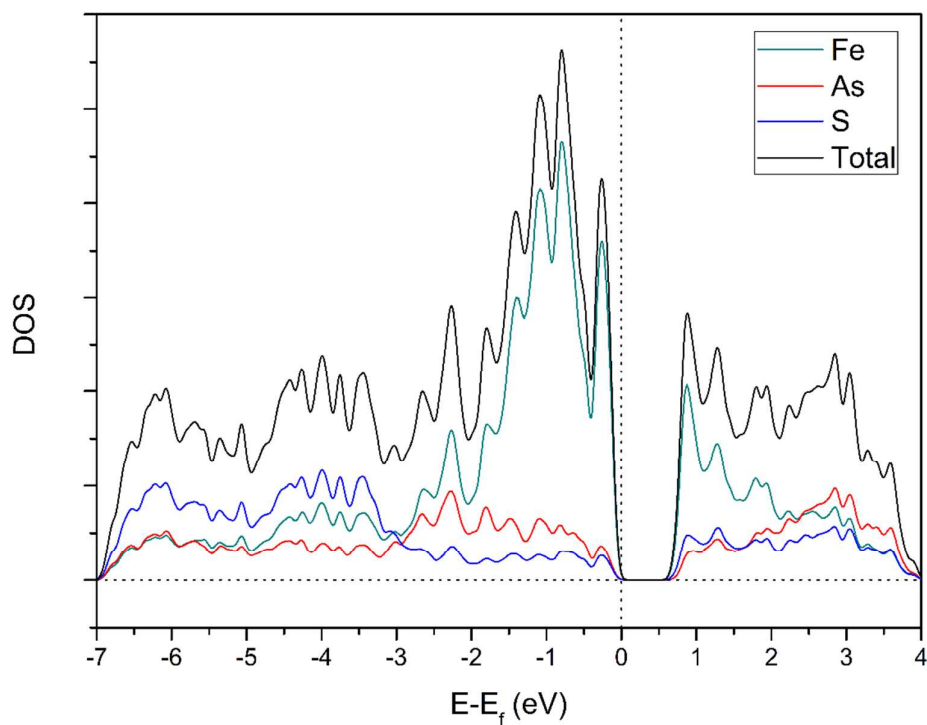


Figure 4: Total and projected DOS over the atoms of arsenopyrite plotted using a Gaussian width of 0.005 Ry.

The electron density map of (010) plane is shown on Figure 5, indicating that the electron density between the neighbor Fe atoms is very small.

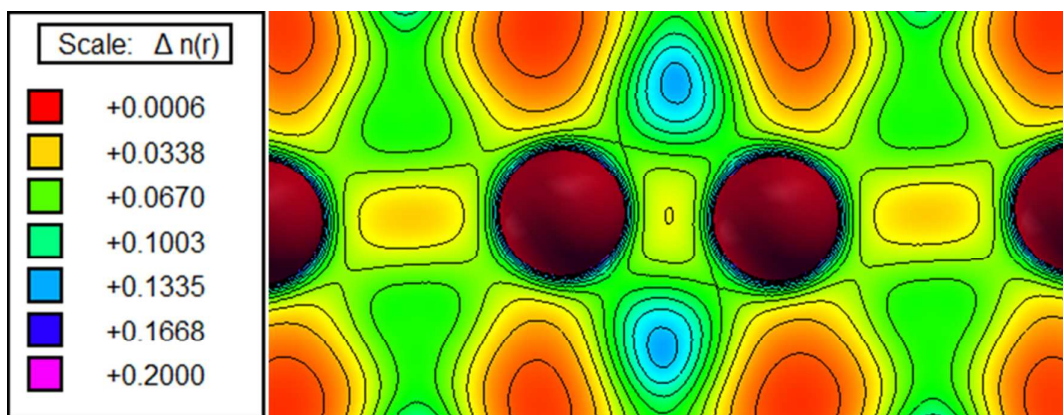


Figure 5: Electronic density map of arsenopyrite (010) plane. Red balls are iron atoms.

QTAIM analysis was performed for arsenopyrite in order to characterize the chemical bonding in the structure. A total of 90 critical points were found,

with 24 of them being nonequivalent: 3 nuclei critical points (NCP), 7 bond critical points (BCP), 9 ring critical points (RCP) and 5 cage critical points (CCP). Their positions are shown in Figure 6 and the respective data are shown on Table 3 (a complete table is shown at Table S2). The Morse relationship ensures that $n - b + r - c = 0$, with $n, c \geq 1$, and $b, r \geq 3$ which holds for the nonequivalent points.

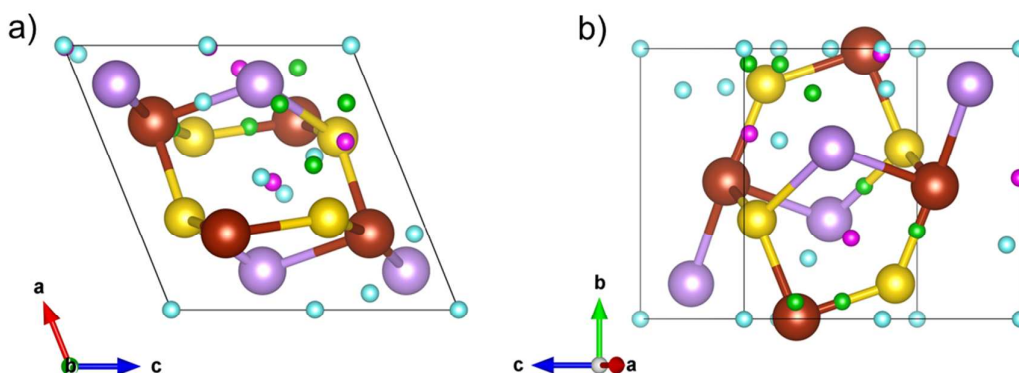


Figure 6: Bond critical points (BCP) in green, Ring critical points (RCP) in blue, and Cage critical points (CCP) in pink for arsenopyrite QTAIM analysis. Atoms in red are iron, in yellow are sulfur and in purple are arsenic.

Table 3: Critical points in QTAIM analysis.

| Critical points | $\rho(r_c)$ * | $\nabla^2\rho(r_c)$ * | Chemical meaning |
|-----------------|---------------|-----------------------|------------------|
| Fe | 6.2235 | -73.0292 | |
| As | 0.5412 | -18.0058 | |
| S | 0.3588 | -10.8180 | |
| b1 | 0.0721 | 0.0492 | Fe-As |
| b2 | 0.0961 | 0.1501 | Fe-S |
| b3 | 0.0733 | 0.0730 | Fe-As |
| b4 | 0.0924 | 0.1996 | Fe-S |
| b5 | 0.0725 | 0.0475 | Fe-As |
| b6 | 0.0828 | -0.0075 | As-S |
| b7 | 0.0881 | 0.2232 | Fe-S |
| r1 | 0.0326 | 0.0546 | Fe...Fe long |
| r2 | 0.0430 | 0.0539 | Fe...Fe short |

* In atomic units.

Concerning the BCPs, three are Fe–S bonds, three Fe–As bonds and one As–S bond, as shown in Figure 7a. The critical points involving Fe–S bonds have positive Laplacian indicating larger ionic character. Schmokel *et al.* [52] have proposed that Fe-S bond in pyrite and marcasite have some covalent character due to Fe *d* orbitals mixing involved in this bond. The Fe–S BCP shows values of density and Laplacian (see Table 3) close to those of Gibbs *et al.* [60] calculated using DFT/LDA and localized basis sets and also close to the values published by Schmokel *et al.* [52] in a DFT/PBE study using multipole refinement. Aray *et al.* [61] found a value of 0.079 a.u. of density for the Fe–S BCP in pyrite and 0.13251 a.u. for the S–S BCP in DFT/PBE (FP-LAPW, full-potential linearized augmented plane-wave + local orbitals) calculations. The Fe-As BCP has density and positive laplacian smaller than the Fe-S BCP indicating that Fe-S has larger ionic character and is stronger than the Fe-As bonding. The As–S BCP has density of 0.0828 a.u. and Laplacian of -0.0075, which means it has covalent character. Schmokel *et al.* [52] found similar results for density and laplacian of S–S BCP in pyrite and marcasite. The electron density and laplacian of the S-S BCP in marcasite is 0.115 a.u. and -0.015 a.u., respectively, compared to the values of the same bond in pyrite of 0.126 a.u. and -0.043 a.u., respectively, indicate that this bond is stronger in pyrite than in marcasite. This result is similar to the density of S-S BCP in covellite (0.135 a.u.) and its laplacian (-0.079 a.u.) found by Morales-García [62] using similar computational method. Comparing with our results for As–S BCP in arsenopyrite of 0.083 and -0.007 a.u. for density and laplacian, respectively, it is expected that the As–S bond in arsenopyrite is weaker than the S–S bond in pyrite, marcasite and covellite. However, analyzing the values shown in Table 3, the As–S bond is the strongest in arsenopyrite and, therefore, unlikely to break in surface cleavage.

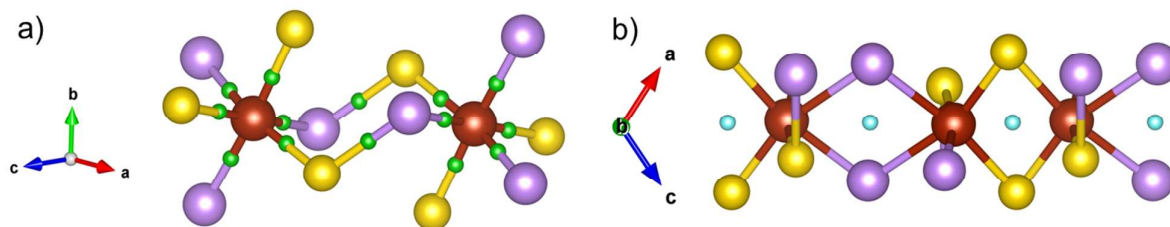


Figure 7: a) Bond critical points and b) Ring critical points in detail. Yellow atoms are sulfur, purple are arsenic and red are iron.

The ELF (Electron Localization Function) map was generated (Figure 8) for the As-S bond. In the region where the ELF value is close to 1, the electrons are localized, and in the regions where they are delocalized, like a homogeneous electron gas, as in metallic bonding, it has a value of 0.5. In Figure 8, it is possible to see the shared cloud between As and S atoms, indicating a covalent bond.

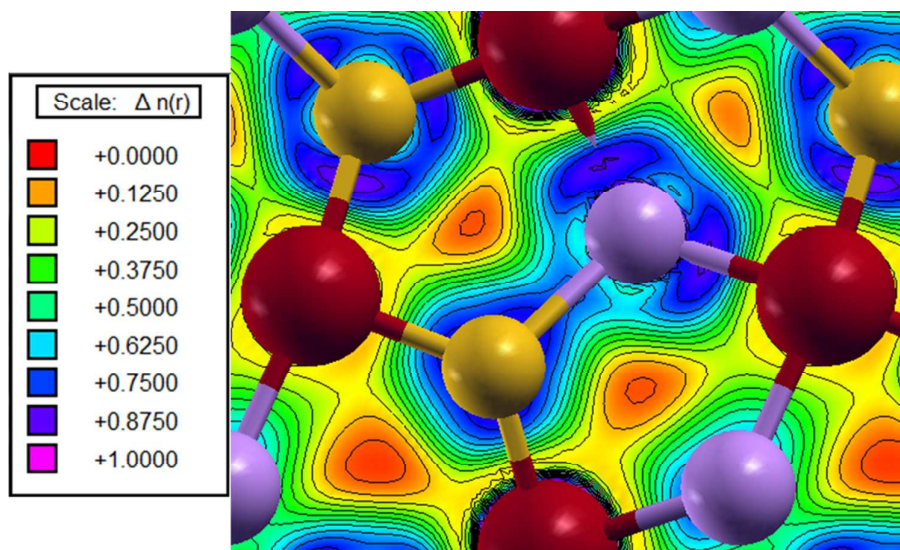


Figure 8: ELF of arsenopyrite As-S bond. Red is iron, purple is arsenic and yellow is sulfur.

In the QTAIM analysis no evidence of Fe–Fe bond has been found in arsenopyrite. A ring critical point (RCP) between two iron neighbor atoms was found as expected, see Figure 7b. From our QTAIM analysis the hypothesis of the Fe–Fe bond is completely discharged. The values of density and laplacian for the r1 and r2 RCPs corresponding to the Fe...Fe distances of 3.765 and

2.668 Å are very similar and the interaction of these atoms must have the same nature. The ELF map was generated (Figure 9) for the Fe-Fe region. The ELF value between two Fe atoms is estimated to be 0.25, which is not characteristic of chemical bonding.

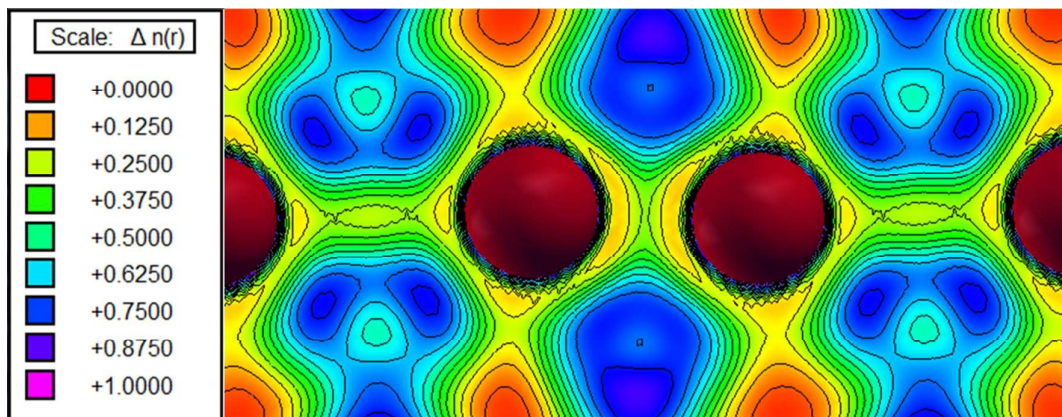


Figure 9: ELF of arsenopyrite (010) plane. Red ball is iron.

The calculated atomic charges and volumes in QTAIM are resumed in Table 4. The estimated positive atomic charge for As is reasonable since sulfur is more electronegative. The integration of the AsS basins lead to $-0.41e$ and $0.41e$ for the iron basin. This is coherent with the $Fe^{2+}(AsS)^{2-}$. The As and S atoms have the largest volumes, which means that these atoms dominate the crystal compressibility.

Table 4: Atomic charges in AIM analysis

| Atoms | Charge | Volume (u.a.) | Pauling's Electronegativity |
|-------|--------|---------------|-----------------------------|
| Fe | 0.41 | 69.9 | 1.83 |
| As | 0.18 | 112.9 | 2.18 |
| S | -0.59 | 111.8 | 2.58 |
| Total | | 1178.5 | |

The c parameter [63] can be used to evaluate the difference between topological charge, $Q(\Omega)$, and nominal oxidation state, $OS(\Omega)$, according to equation (1) and it indicates the ionicity of the crystal.

$$c = \frac{1}{N} \sum_{\Omega=1}^N \frac{Q(\Omega)}{OS(\Omega)} \quad (1)$$

The closest to 1 is c , more ionic is the crystal and the closest to 0, more covalent. The value of c for arsenopyrite is 0.205 taking $\text{Fe}^{2+}\text{As}^{1-}\text{S}^{1-}$ oxidation numbers as reference, which indicates a solid that presents large covalent character.

The bulk modulus of arsenopyrite was calculated and compared with experimental and theoretical values of other compounds, as shown on Table 5. Our value of 147.5 GPa is 15 GPa greater than the experimental value obtained by Fan *et al.* [64] in X-ray diffraction in the pressure range from 0 to 9.6 GPa. The calculated and experimental values for marcasite and pyrite are in the same level of magnitude of our result. This shows that the method used in this work describes well not just each atom individually, but also the whole crystal structure.

Table 5: Calculated and experimental bulk moduli for arsenopyrite, marcasite and pyrite.

| Compound | Bulk modulus (GPa) | Reference |
|--------------|--------------------|------------------------|
| Arsenopyrite | 147.5 | This work |
| Arsenopyrite | 133 | X-ray diffraction [64] |
| Marcasite | 150.1 | PBE/plane waves [43] |
| Marcasite | 146.5 | X-ray diffraction [65] |
| Pyrite | 150 | PAW/plane waves [66] |
| Pyrite | 143 | X-ray diffraction [67] |

Surface

To the best of our knowledge, there is no consensus in the literature concerning the favored arsenopyrite cleavage. The (100) [11], (001) [30], (101) [25, 31] and (110) [21, 32] surfaces have been indicated by different references as most favorable to be cleaved. It is important to highlight that in some of these works the unit cell used to define the Miller indices was not clearly indicated explaining part of this divergence. The Table S1 shows the correspondence

between the $C2_1/d$ and $P2_1/c$ unit cells which are normally used to describe arsenopyrite. We stress that it is important to clearly define the unit cell used to define the surfaces.

Several surfaces were created based on the $P2_1/c$ optimized bulk cell to compare their energies and the planes are shown on Figure S3. The non-optimized structures are presented on Figure S4. All the different terminations were calculated. All of them are type II of Tasker [68], namely, they had charged layers formed by cations and anions symmetrically arranged in a way that the charges cancel on the surface and they do not have a resultant dipole perpendicular to the surface. Usually, this means that there is no reconstruction of these surfaces, only relaxation. The surface energy was calculated according to equation (2) [69]:

$$\Delta E_{\text{surface}}^n = \frac{(E^n - nE_{\text{bulk}})}{2A}; \quad (2)$$

where E^n is the energy of a n -layer slab, E_{bulk} is the energy of the unit cell which correspond to a single layer, and A is the surface area. The cleavage energy (E_{cleav}) was calculated before the relaxation, in a single point calculation, and the surface energy (E_{surf}) was calculated after the relaxation. The results are shown on Table 6 together with the coordination of each surface atom in the different cleavages. Figure 10 shows the structures after relaxation.

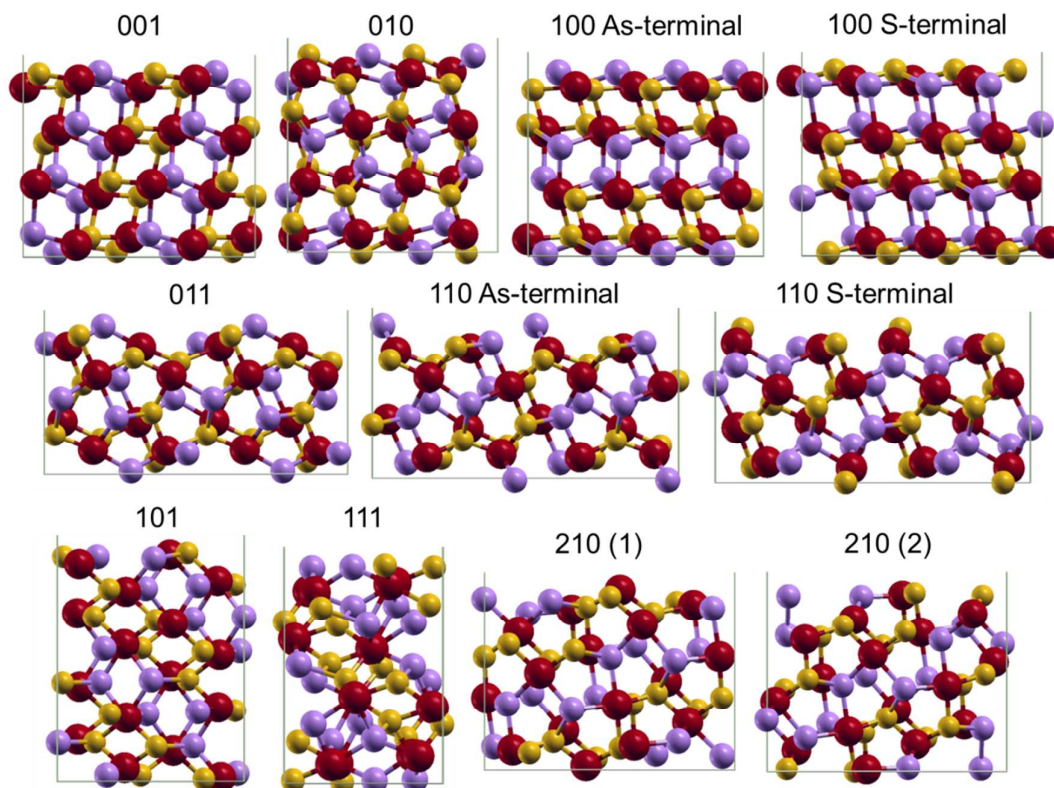


Figure 10: Optimized arsenopyrite surfaces. Iron is in red, sulfur in yellow and arsenic in purple. Miller indices are based on the $P2_1/c$ symmetry.

As one can see at Table 6, the surface and cleavage energies are related to the number of bonds broken. The (001), (010), and (100) planes are the most favored cleavage surfaces with E_{surf} between 1.05 and 1.09 Jm^{-2} and E_{cleav} between 1.21 and 1.35 Jm^{-2} . The (100) plane is more likely to cleave on the As-terminal surface. The top view of these planes is presented on Figure 11, which shows that (001) and (100) surfaces expose a similar terminal structure. In these planes no As–S bond is broken, as expected. The other ones have higher energies and are unlikely to be cleaved. Nevertheless, they may be exposed when fractured due to twinning along the high cleavage energy planes. According to Klein *et al.* [25], twinning appear on surfaces (100) and (001) of the $P2_1/c$ cell, whereas according to Dana and Ford [32] it appears on surfaces (110) and (101).

Table 6: Surface energies and coordination of surface atoms of different arsenopyrite surfaces.

| Surface | Surface Energy/J m ⁻² | Cleavage Energy/J m ⁻² | Coordination | | |
|-----------------|----------------------------------|-----------------------------------|--------------|------|------|
| | | | Fe | As | S |
| Bulk | - | - | 6 | 4 | 4 |
| 001 | 1.05 | 1.23 | 5 | 3 | 3 |
| 010 | 1.06 | 1.28 | 5 | 3 | 3 |
| 100 As-terminal | 1.07 | 1.21 | 5 | 3 | 4 |
| 100 S-terminal | 1.09 | 1.35 | 5 | 4 | 4 |
| 011 | 1.30 | 1.50 | 5, 4 | 2 | 3 |
| 101 | 1.47 | 1.65 | 4 | 3 | 3 |
| 110 S-terminal | 1.52 | 1.91 | 4 | 3 | 3, 2 |
| 110 As-terminal | 1.57 | 1.93 | 4 | 3, 2 | 3 |
| 111 | 1.51 | 1.78 | 5 | 2 | 2 |
| 210 (1) | 1.44 | 1.59 | 4, 3 | 3, 2 | 4, 3 |
| 210 (2) | 1.78 | 2.29 | 4, 3 | 3, 1 | 2 |

Pyrite has a cubic unit cell, then the (100), (010), and (001) surfaces are equivalent and have been used in adsorption or oxidation studies of pyrite [14, 16]. Hung *et al.* [12, 13] have studied pyrite's (100), (110), (111), and (210) surfaces through PBE/plane waves calculations. Their results follow the same tendency of arsenopyrite, except for the high value in (100) cleavage energy of 4.25 J m⁻². Table 7 shows a comparison between the surface and cleavage energies for arsenopyrite and pyrite. However, it is important to note that pyrite and arsenopyrite present different unit cells, therefore the bond breaking in the surface formation is different.

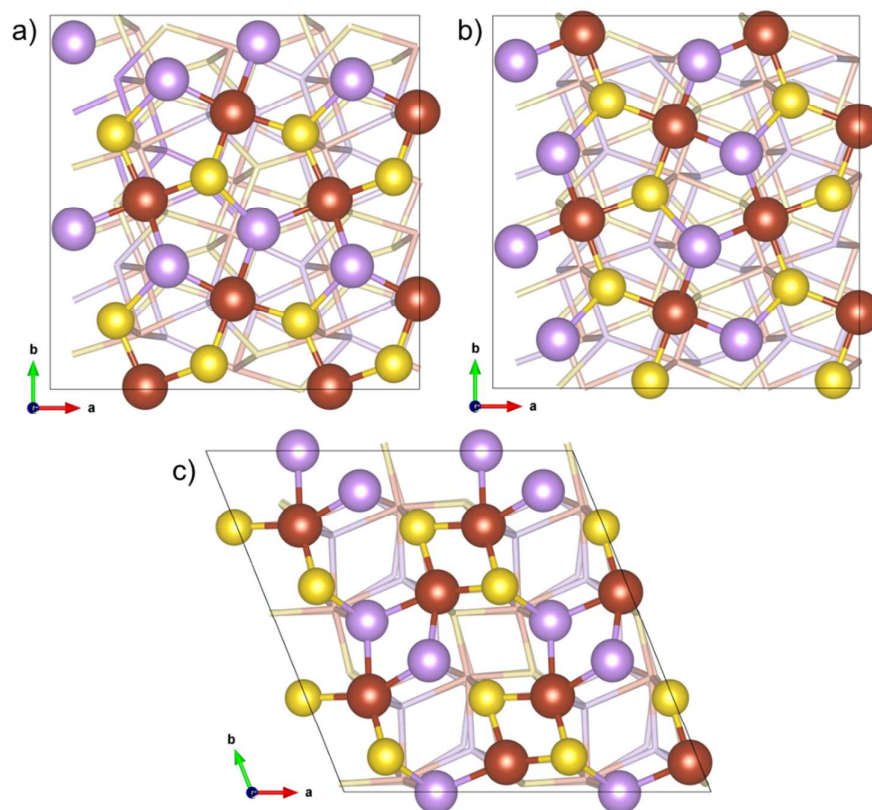


Figure 11: Top view of surfaces: a) (001); b) (100); c) (010). Red is iron, purple is As and yellow is sulfur.

Table 7: Comparison of Arsenopyrite and Pyrite's surface energies.

| Surface | Arsenopyrite | | Pyrite [12, 13] | |
|----------------------|----------------------------------|-----------------------------------|----------------------------------|-----------------------------------|
| | Surface Energy/J m ⁻² | Cleavage Energy/J m ⁻² | Surface Energy/J m ⁻² | Cleavage Energy/J m ⁻² |
| 001 | 1.05 | 1.23 | | |
| 010 | 1.06 | 1.28 | 1.06 ³ | 4.25 ³ |
| 100 | 1.07 | 1.21 | | |
| 110 (S-terminal) | 1.52 | 1.91 | 1.68 | 1.85 |
| 110 (As-terminal) | 1.57 | 1.93 | 1.54 ¹ | 1.74 ¹ |
| 110 (1) ² | 1.76 | 2.08 | - | - |
| 110 (2) ² | 2.08 | 2.40 | - | - |
| 111 | 1.51 | 1.78 | 1.40 | 1.61 |
| 210 | 1.44 | 1.59 | 1.50 | 1.74 |

¹Microfaceted (110) pyrite surface.

²Corkhill *et al.* [21].

³The (001), (010) and (100) pyrite surfaces are equivalent.

Corkhill *et al.* [21] also calculated the E_{surf} and E_{cleav} of (110) arsenopyrite surfaces in two different terminations using PBE/plane waves. The models used by them (24 atoms, $5.65 \text{ \AA} \times 7.91 \text{ \AA} \times 16.9 \text{ \AA}$ cell) are four times smaller than the ones considered in the present work and do not have equal terminations on top and bottom surfaces. Their estimated values of E_{surf} (1.76 and 2.08 J m^{-2}), and E_{cleav} (2.08 and 2.40 J m^{-2}) are higher than our results, both presented on Table 7.

The largest change in the relaxed slab model was observed for the surface atoms with values of 0.12 \AA for Fe–As bond on the (100) surface, 0.14 \AA for Fe–As bond on the (001) surface, and 0.14 \AA for Fe–Fe distance on the (010) surface.

The projected DOS over the surface atoms of (001), (010), and (100) planes are shown in Figure 12. Similarly to the bulk, the Fe $3d$ orbitals are dominant around the Fermi level, which means that nucleophilic or electrophilic interactions with adsorbents are most likely to occur on this atom. For all surfaces, the band gap that was present on the bulk almost disappeared.

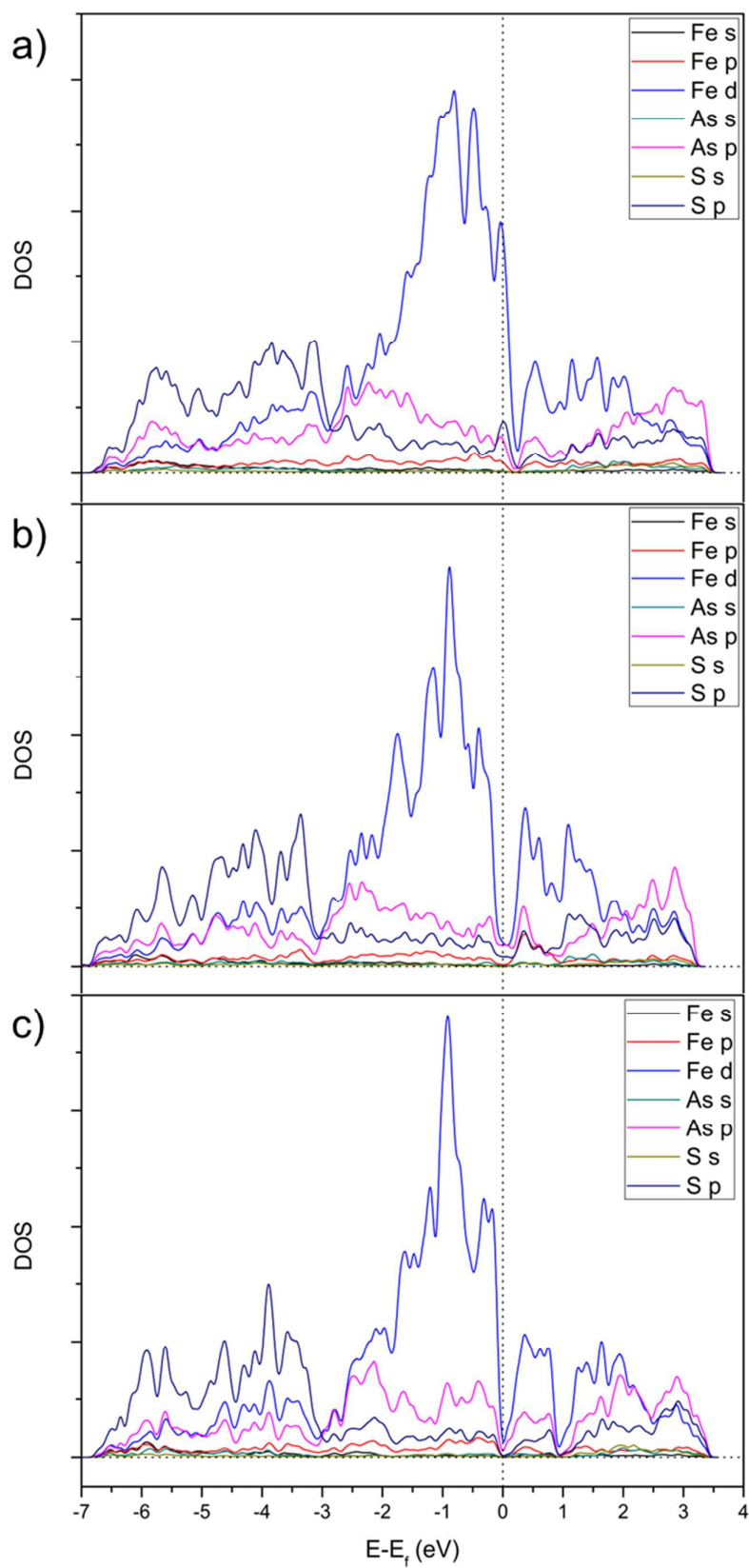


Figure 12: Projected DOS over the atoms of the surfaces: a) (001); b) (010); c) (100) plotted using a Gaussian width of 0.005 Ry.

4. Conclusion

The structural and electronic properties of the arsenopyrite and its different cleavage surfaces have been investigated by DFT/plane waves method. For the arsenopyrite bulk, the structural parameters are in good agreement with the experimental data and previously reported calculated values. The Bader's QTAIM analysis indicates that there is no Fe–Fe bond in arsenopyrite. Only a ring critical bond was found between the two Fe atoms. The As–S bond has covalent character and the Fe–As and Fe–S bonds have ionic character. In agreement to the previously reported calculations of covellite, pyrite and marcasite, which concluded that S–S bond is unlikely to be broken, the As–S bond is also unlikely to be broken in the cleavage. The surface and cleavage energies have been estimated for different surfaces. The (001), (010) and (100) are considered the most favored cleavage planes, with surface energies close to 1.07 J m^{-2} . In these three surfaces the As-S bond is not broken and the Fe, As and S are exposed in the surface. The (001), (010) and (100) surfaces are adequate models for investigating the surface reactivity of arsenopyrite. The projected DOS on the surface show that the valence and conduction bands close to the Fermi level are mostly due to the *d*-orbitals of iron atoms indicating that this atom is the preferred site for adsorption and, hence, must be involved in the initial steps of the arsenopyrite oxidation. The surface oxidation of arsenopyrite is presently being investigated in our laboratory.

Electronic Supplementary Information (ESI): Table with the surfaces correspondence in C21/d and P21/c unit cells, QTAIM critical points, the k-points used for band calculations, project DOS over the arsenopyrite atoms and the cleavage surfaces are available. This material is available free of charge via the Internet at <http://>.

Acknowledgments: The support of the Brazilian agencies Fundação de Amparo à Pesquisa do Estado de Minas Gerais (FAPEMIG), Conselho Nacional para o Desenvolvimento Científico e Tecnológico (CNPq) and Coordenação de Aperfeiçoamento de Pessoal de Ensino Superior (CAPES) are

also gratefully acknowledged. The National Institute of Science and Technology for Mineral Resources, Water and Biodiversity has also supported this work – INCT-ACQUA (<http://www.acqua-inct.org>).

5. References

1. Nesbitt, H.W., I.J. Muir, and A.R. Prarr, *Oxidation of arsenopyrite by air and air-saturated, distilled water, and implications for mechanism of oxidation*. *Geochimica et Cosmochimica Acta*, 1995. **59**(9): p. 1773-1786.
2. Corkhill, C.L. and D.J. Vaughan, *Arsenopyrite oxidation – A review*. *Applied Geochemistry*, 2009. **24**(12): p. 2342-2361.
3. Rull, F., et al., *Spectroscopic Raman study of sulphate precipitation sequence in Rio Tinto mining district (SW Spain)*. *Environmental Science and Pollution Research*, 2014. **21**(11): p. 6783-6792.
4. Akcil, A. and S. Koldas, *Acid Mine Drainage (AMD): causes, treatment and case studies*. *Journal of Cleaner Production*, 2006. **14**(12-13): p. 1139-1145.
5. Cheng, H.F., et al., *Geochemical processes controlling fate and transport of arsenic in acid mine drainage (AMD) and natural systems*. *Journal of Hazardous Materials*, 2009. **165**(1-3): p. 13-26.
6. Buckley, A.N. and G.W. Walker, *The Surface-Composition of Arsenopyrite Exposed to Oxidizing Environments*. *Applied Surface Science*, 1988. **35**(2): p. 227-240.
7. Fernandez, P.G., H.G. Linge, and M.W. Wadsley, *Oxidation of arsenopyrite (FeAsS) in acid .1. Reactivity of arsenopyrite*. *Journal of Applied Electrochemistry*, 1996. **26**(6): p. 575-583.
8. Nesbitt, H.W. and I.J. Muir, *Oxidation states and speciation of secondary products on pyrite and arsenopyrite reacted with mine waste waters and air*. *Mineralogy and Petrology*, 1998. **62**(1-2): p. 123-144.
9. Almeida, C.M.V.B. and B.F. Giannetti, *Electrochemical study of arsenopyrite weathering*. *Physical Chemistry Chemical Physics*, 2003. **5**(3): p. 604-610.
10. Mikhlin, Y.L., A.S. Romanchenko, and I.P. Asanov, *Oxidation of arsenopyrite and deposition of gold on the oxidized surfaces: A scanning probe microscopy, tunneling spectroscopy and XPS study*. *Geochimica et Cosmochimica Acta*, 2006. **70**(19): p. 4874-4888.
11. Corkhill, C.L., et al., *The oxidative dissolution of arsenopyrite (FeAsS) and enargite (Cu₃AsS₄) by *Leptospirillum ferrooxidans**. *Geochimica et Cosmochimica Acta*, 2008. **72**(23): p. 5616-5633.
12. Hung, A., et al., *Density-functional theory studies of pyrite FeS₂(100) and (110) surfaces*. *Surface Science*, 2002. **513**(3): p. 511-524.
13. Hung, A., et al., *Density-functional theory studies of pyrite FeS₂ (111) and (210) surfaces*. *Surface Science*, 2002. **520**(1-2): p. 111-119.
14. Stirling, A., M. Bernasconi, and M. Parrinello, *Ab initio simulation of water interaction with the (100) surface of pyrite*. *Journal of Chemical Physics*, 2003. **118**(19): p. 8917-8926.
15. Stirling, A., M. Bernasconi, and M. Parrinello, *Defective pyrite (100) surface: An ab initio study*. *Physical Review B*, 2007. **75**(16): p. 165406.

16. Sit, P.H.L., M.H. Cohen, and A. Selloni, *Interaction of Oxygen and Water with the (100) Surface of Pyrite: Mechanism of Sulfur Oxidation*. Journal of Physical Chemistry Letters, 2012. **3**(17): p. 2409-2414.
17. de Oliveira, C. and H.A. Duarte, *Disulphide and metal sulphide formation on the reconstructed (001) surface of chalcopyrite: A DFT study*. Applied Surface Science, 2010. **257**(4): p. 1319-1324.
18. de Lima, G.F., et al., *Water Adsorption on the Reconstructed (001) Chalcopyrite Surfaces*. The Journal of Physical Chemistry C, 2011. **115**(21): p. 10709-10717.
19. de Oliveira, C., et al., *Reconstruction of the Chalcopyrite Surfaces—A DFT Study*. The Journal of Physical Chemistry C, 2012. **116**(10): p. 6357-6366.
20. de Lima, G.F., et al., *Sulfuric and hydrochloric acid adsorption on the reconstructed sulfur terminated (001) chalcopyrite surface*. International Journal of Quantum Chemistry, 2012. **112**(19): p. 3216-3222.
21. Corkhill, C.L., M.C. Warren, and D.J. Vaughan, *Investigation of the electronic and geometric structures of the (110) surfaces of arsenopyrite (FeAsS) and enargite (Cu₃AsS₄)*. Mineralogical Magazine, 2011. **75**(1): p. 45-63.
22. Reich, M. and U. Becker, *First-principles calculations of the thermodynamic mixing properties of arsenic incorporation into pyrite and marcasite*. Chemical Geology, 2006. **225**(3-4): p. 278-290.
23. Blanchard, M., et al., *Arsenic incorporation into FeS₂ pyrite and its influence on dissolution: A DFT study*. Geochimica et Cosmochimica Acta, 2007. **71**(3): p. 624-630.
24. Pearce, C.I., R.A.D. Patrick, and D.J. Vaughan, *Electrical and Magnetic Properties of Sulfides*. Reviews in Mineralogy and Geochemistry, 2006. **61**(1): p. 127-180.
25. Klein, C., C.S. Hurlbut, and J.D. Dana, *Manual of mineralogy : (after James D. Dana)*. 21st ed. 1999, New York: J. Wiley. xiv, 681 p., 4 p. of col. plates.
26. Fuess, H., et al., *Crystal-Structure Refinement and Electron-Microscopy of Arsenopyrite*. Zeitschrift Fur Kristallographie, 1987. **179**(1-4): p. 335-346.
27. Morimoto, N. and L.A. Clark, *Arsenopyrite Crystal-Chemical Relations*. American Mineralogist, 1961. **46**(11-2): p. 1448-1469.
28. Vaughan, D.J. and J.R. Craig, *Mineral chemistry of metal sulfides*. Cambridge earth science series. 1978, Cambridge Eng. ; New York: Cambridge University Press. xv, 493 p.
29. Bindi, L., et al., *Stoichiometric Arsenopyrite, FeAsS, from La Roche-Baluc Quarry, Loire-Atlantique, France: Crystal Structure and Mossbauer Study*. The Canadian Mineralogist, 2012. **50**(2): p. 471-479.
30. Ford, M. and C.C. Ferguson, *Cleavage Strain in the Variscan Fold Belt, County Cork, Ireland, Estimated from Stretched Arsenopyrite Rosettes*. Journal of Structural Geology, 1985. **7**(2): p. 217-223.
31. Wolff, G.A. and J.D. Broder, *Cleavage and the Identification of Minerals*. American Mineralogist, 1960. **45**(11-2): p. 1230-1242.
32. Dana, E.S. and W.E. Ford, *A Text-book of Mineralogy: With an Extended Treatise on Crystallography and Physical Mineralogy*. 4 ed. 1966, New York: Wiley.
33. Giannozzi, P., et al., *QUANTUM ESPRESSO: a modular and open-source software project for quantum simulations of materials*. Journal of Physics-Condensed Matter, 2009. **21**(39).
34. Perdew, J.P. and Y. Wang, *Accurate and Simple Analytic Representation of the Electron-Gas Correlation-Energy*. Physical Review B, 1992. **45**(23): p. 13244-13249.
35. Vanderbilt, D., *Soft Self-Consistent Pseudopotentials in a Generalized Eigenvalue Formalism*. Physical Review B, 1990. **41**(11): p. 7892-7895.
36. Monkhorst, H.J. and J.D. Pack, *Special Points for Brillouin-Zone Integrations*. Physical Review B, 1976. **13**(12): p. 5188-5192.

37. Marzari, N., et al., *Thermal Contraction and Disorder of the Al(110) Surface*. Physical Review Letters, 1999. **82**(16): p. 3296-3299.
38. Beeman, D., *Some Multistep Methods for Use in Molecular-Dynamics Calculations*. Journal of Computational Physics, 1976. **20**(2): p. 130-139.
39. Parrinello, M. and A. Rahman, *Polymorphic Transitions in Single-Crystals - a New Molecular-Dynamics Method*. Journal of Applied Physics, 1981. **52**(12): p. 7182-7190.
40. Bader, R.F.W., *A quantum theory of molecular structure and its applications*. Chemical Reviews, 1991. **91**(5): p. 893-928.
41. Otero-de-la-Roza, A., et al., *Critic: a new program for the topological analysis of solid-state electron densities*. Computer Physics Communications, 2009. **180**(1): p. 157-166.
42. Otero-de-la-Roza, A., D. Abbasi-Perez, and V. Luana, *GIBBS2: A new version of the quasiharmonic model code. II. Models for solid-state thermodynamics, features and implementation*. Computer Physics Communications, 2011. **182**(10): p. 2232-2248.
43. Gudelli, V.K., et al., *Phase Stability and Thermoelectric Properties of the Mineral FeS₂: An Ab Initio Study*. Journal of Physical Chemistry C, 2013. **117**(41): p. 21120-21131.
44. Hulliger, F. and E. Mooser, *Semiconductivity in pyrite, marcasite and arsenopyrite phases*. Journal of Physics and Chemistry of Solids, 1965. **26**(2): p. 429-433.
45. Pearson, W.B., *Compounds with the marcasite structure*, in *Zeitschrift für Kristallographie - Crystalline Materials*. 1965. p. 449.
46. Nickel, E.H., *Structural stability of minerals with the pyrite, marcasite, arsenopyrite and lollingite structures*. The Canadian Mineralogist, 1968. **9**(3): p. 311-321.
47. Nickel, E.H., *The application of ligand-field concepts to an understanding of the structural stabilities and solid-solution limits of sulphides and related minerals*. Chemical Geology, 1970. **5**(4): p. 233-241.
48. Brostige, G. and A. Kjekshus, *Bonding Schemes for Compounds with Pyrite, Marcasite, and Arsenopyrite Type Structures*. Acta Chemica Scandinavica, 1970. **24**(8): p. 2993-&.
49. Goodenou, Jb., *Energy-Bands in TX₂ Compounds with Pyrite, Marcasite, and Arsenopyrite Structures*. Journal of Solid State Chemistry, 1972. **5**(1): p. 144-&.
50. Pauling, L., *Metal-Metal Bond Lengths in Complexes of Transition-Metals*. Proceedings of the National Academy of Sciences of the United States of America, 1976. **73**(12): p. 4290-4293.
51. Tossell, J.A., D.J. Vaughan, and J.K. Burdett, *Pyrite, marcasite, and arsenopyrite type minerals: Crystal chemical and structural principles*. Physics and Chemistry of Minerals, 1981. **7**(4): p. 177-184.
52. Schmokel, M.S., et al., *Atomic properties and chemical bonding in the pyrite and marcasite polymorphs of FeS₂: a combined experimental and theoretical electron density study*. Chemical Science, 2014. **5**(4): p. 1408-1421.
53. Jones, R.A. and H.W. Nesbitt, *XPS evidence for Fe and As oxidation states and electronic states in loellingite (FeAs₂)*. American Mineralogist, 2002. **87**(11-12): p. 1692-1698.
54. Setyawan, W. and S. Curtarolo, *High-throughput electronic band structure calculations: Challenges and tools*. Computational Materials Science, 2010. **49**(2): p. 299-312.
55. Vaughan, D.J., *Sulfide Mineralogy and Geochemistry: Introduction and Overview*. Reviews in Mineralogy and Geochemistry, 2006. **61**(1): p. 147.
56. Tran, F. and P. Blaha, *Accurate Band Gaps of Semiconductors and Insulators with a Semilocal Exchange-Correlation Potential*. Physical Review Letters, 2009. **102**(22): p. 226401.
57. Ferrer, I.J., et al., *About the band gap nature of FeS₂ as determined from optical and photoelectrochemical measurements*. Solid State Communications, 1990. **74**(9): p. 913-916.
58. Ennaoui, A., et al., *Iron disulfide for solar energy conversion*. Solar Energy Materials and Solar Cells, 1993. **29**(4): p. 289-370.

59. Opahle, I., K. Koepernik, and H. Eschrig, *Full-potential band-structure calculation of iron pyrite*. Physical Review B, 1999. **60**(20): p. 14035-14041.
60. Gibbs, G.V., et al., *Theoretical Electron Density Distributions for Fe- and Cu-Sulfide Earth Materials: A Connection between Bond Length, Bond Critical Point Properties, Local Energy Densities, and Bonded Interactions*. The Journal of Physical Chemistry B, 2007. **111**(8): p. 1923-1931.
61. Aray, Y., et al., *Correlation of the Topology of the Electron Density of Pyrite-Type Transition Metal Sulfides with Their Catalytic Activity in Hydrodesulfurization*. Angewandte Chemie International Edition, 2000. **39**(21): p. 3810-3813.
62. Morales-García, A., et al., *First-Principles Calculations and Electron Density Topological Analysis of Covellite (CuS)*. The Journal of Physical Chemistry A, 2014.
63. Mori-Sánchez, P., A.M. Pendás, and V. Luaña, *A Classification of Covalent, Ionic, and Metallic Solids Based on the Electron Density*. Journal of the American Chemical Society, 2002. **124**(49): p. 14721-14723.
64. Fan, D.W., et al., *X-ray diffraction study of arsenopyrite at high pressure*. Physics and Chemistry of Minerals, 2011. **38**(2): p. 95-99.
65. Chattopadhyay, T. and H.G. Vonschnering, *High pressure X-ray diffraction study on p -FeS₂, m -FeS₂ and MnS₂ to 340 kbar: A possible high spin-low spin transition in MnS₂*. Journal of Physics and Chemistry of Solids, 1985. **46**(1): p. 113-116.
66. Le Page, Y. and J.R. Rodgers, *Ab initio elasticity of FeS₂ pyrite from 0 to 135 GPa*. Physics and Chemistry of Minerals, 2005. **32**(8-9): p. 564-567.
67. Merkel, S., et al., *Equation of state, elasticity, and shear strength of pyrite under high pressure*. Physics and Chemistry of Minerals, 2002. **29**(1): p. 1-9.
68. Tasker, P.W., *The stability of ionic crystal surfaces*. Journal of Physics C: Solid State Physics, 1979. **12**(22): p. 4977.
69. Dovesi, R., et al., *Ab Initio Quantum Simulation in Solid State Chemistry*, in *Reviews in Computational Chemistry*. 2005, John Wiley & Sons, Inc. p. 1-125.